Analysis and Characterization of Phase Evolution of Nanosized BaTiO$_3$ Powder Synthesized Through a Chemically Modified Sol-Gel Process

ROUHOLAH ASHIRI

In the current research, a cost-effective and modified method with a high degree of reproducibility was proposed for the preparation of fine nanoscale and high-purity BaTiO$_3$. In contrast to the other established methods, in this research, carbonate-free BaTiO$_3$ nanopowders were prepared at a lower temperature and in a shorter time span. To reach an in-depth understanding of the scientific basis of the proposed process, an in-detail analysis was carried out for characterization of nanoscale BaTiO$_3$ particles *via* differential thermal analysis (DTA)/thermogravimetric analysis (TGA), Fourier transform infrared spectroscopy (FTIR), X-ray diffraction (XRD), scanning electron microscopy (SEM), and transmission electron microscopy (TEM) techniques aided by theoretical calculations. The effects of the temperature and time of calcination process on the preparation mechanism, phase transformation, tetragonality, and particle size of BaTiO$_3$ were examined. The reaction that results in the formation of barium titanate initiated at approximately 873 K (600 °C) and seemed to be completed at approximately 1073 K (800 °C) and the polymorphic transformation of cubic to tetragonal initiated at approximately 1173 K (900 °C). It seemed to be completed at approximately 1373 K (1100 °C). According to the reaction mechanism, the formation of BaTiO$_3$ in the initial stage of the interfacial reaction between BaCO$_3$ and TiO$_2$ depends on the BaCO$_3$ decomposition. In the second stage, the BaTiO$_3$ formation is controlled by barium diffusion through the barium titanate layer. In this stage, in contrast to the literature, no secondary phase was detected. The overall characterizations showed the temperature is more effective than time on the progress in process of preparation because of its diffusion-controlled nature.

I. INTRODUCTION

THE demands for high-quality electronic ceramics increase rapidly and the physical properties of materials as they progress from the bulk to the nanoscale regime (1 to 100 nm) continue to be of immense interest and increasing importance for future technological applications. Nanocrystals display properties that are generally found to be scientifically different from the bulk material or the atomic or molecular species from which they can be derived.[1] The properties of the nanocrystals frequently are better than traditional bulk materials that have led to an increase in tendency for preparation of this type of materials by using of economic processes. Indeed, the economic consideration of mass production of nanocrystals is a major issue concerning the research and development.

The ferroelectric nature of nanocrystals occurs because the center of mass of all the negative ions does not coincide with the center of mass of the positive ions, resulting in spontaneous electric polarization.[2] Ferroelectric materials have been under investigation because the stable polarization states could be used to encode the 0 and 1 of the Boolean algebra that form the basis of memory and logic circuitry (FRAM).[1] The rapid advances in the miniaturization of electromagnetic devices have led to a particular need for ceramics with tunable dielectric constants and low losses at microwave frequencies. Ferroelectric materials possess significant tenability, *i.e.*, change of dielectric constant under applied electric field.[3] Among the ferroelectrics, barium titanate is a well-known compound that has been widely used both in academic research and industrial product in the last decades. Barium titanate (BaTiO$_3$) has been used extensively in the manufacture of electronic applications, such as piezoceramic devices, electro-optic elements, high-permittivity ceramic capacitors, positive temperature coefficient resistors, transducers,[4] tunable phase shifters[3] thermistors, gas, temperature and humidity sensors infrared detectors, ferroelectric memories,[5,6] and printed circuit boards.[2] In recent years, high-performance multilayer ceramic capacitors (MLCCs) have developed a toward smaller size and higher capacity, resulting in thinner (below1 μm) green sheets required to produce

ROUHOLAH ASHIRI, formerly Graduate Student, Department of Materials Science and Engineering, Sharif University of Technology, P.O. Box 11365-9466, Tehran, Iran, is now a first-year Ph.D. Student, Department of Materials Engineering, Isfahan University of Technology, P.O. Box 84156-83111, Isfahan, Iran, and Lecturer, Department of Materials Science and Engineering, Dezful Branch, Islamic Azad University, P.O. Box 313, Dezful, Iran. Contact e-mail: ro_ashiri@yahoo.com

MLCCs. These high-performance multilayer ceramic capacitors recently are commercialized by $BaTiO_3$ nano-powders (200 nm size).[7] Miniaturization requires down-sizing of raw materials[8]; consequently, high-purity, nanosized barium titanate powders are required to meet the preceding requirements.

The successful synthesis of barium titanate nanopow-ders with their unique dielectric properties largely depends on the purity and crystal structure. Two major approaches are generally considered for manufacturing $BaTiO_3$ nanoparticles: traditional and advanced pro-cessing. Titanates are conventionally synthesized by solid-state reaction at high temperatures resulting in a wide grain size distribution, multiple phases, and inevitably some degree of porosity. These results are caused by the impurity and inhomogeneity associated with the powder processing stage. The familiar wet chemical routes including the precipitation method, hydrothermal law, microemulsion approach, and sol-gel process have been developed to offer many advan-tages.[9] In particular, the low-temperature sol-gel process offer an exciting possibility for the synthesis of high-purity, homogeneous, ultrafine, and multicompo-nent powders through which electronic components with tailored and predictable properties can be prepared.[10]

In the current research, a chemically modified method was applied to prepare nanoscale $BaTiO_3$ particles that can be carried out at lower temperatures to obtain a product free from secondary phases or impurities. In contrast, an elaborated explanation regarding the mech-anism of synthesis and phase development is not available in the literature. The formation mechanism of barium titanate nanopowders from a gel-derived precursor is complicated. Moreover, a mechanism is strongly dependent on the preparation route. Few publications address the path of thermally induced changes occur during sol-gel-powder transformation. In the current work, the objective is to investigate the phase evolution of barium titanate from alkoxide gel-derived precursor *via* thermal analysis. Fourier transform infra-red spectroscopy (FTIR), differential thermal analysis (DTA)/thermogravimetric analysis (TGA), X-ray dif-fraction (XRD), scanning electron microscopy (SEM), and transmission electron microscopy (TEM) investiga-tions were used to study and analyze the mechanism of synthesis and to characterize the structure evolution during synthesis process.

II. EXPERIMENTAL

A. Sample Preparation

To synthesize $BaTiO_3$ nanoparticles, a modified sol-gel route was adopted and a two-step hydrolysis process was employed. In this process, a low-temperature hydrolysis (LTH), lower molar ratio of acetic acid, and 2-propanol and higher molar ratio of deionized water were used. Unlike other synthesis routes,[11] no modifier such as acetyl acetone was used as a precursor in this study.

A modified acetate derived $BaTiO_3$ sol was prepared by using the glacial acetic acid (assay 100 pct; Merck,

Whitehouse Station, NJ), barium acetate (assay > 99 pct; Merck), titanium tetraisopropyl alkoxide or TTIP, (assay > 98 pct; Merck), 2-propanol (assay > 99 pct; Merck), and deionized water as precursors. The optimal formulation of sol consists of acetic acid, barium acetate, TTIP, 2-propanol, and deionized water with 6:1:1:1:150 molar ratios, respectively. The method of preparation of nanoscale powders and the tempera-ture at each step of preparation is summarized in Figure 1.
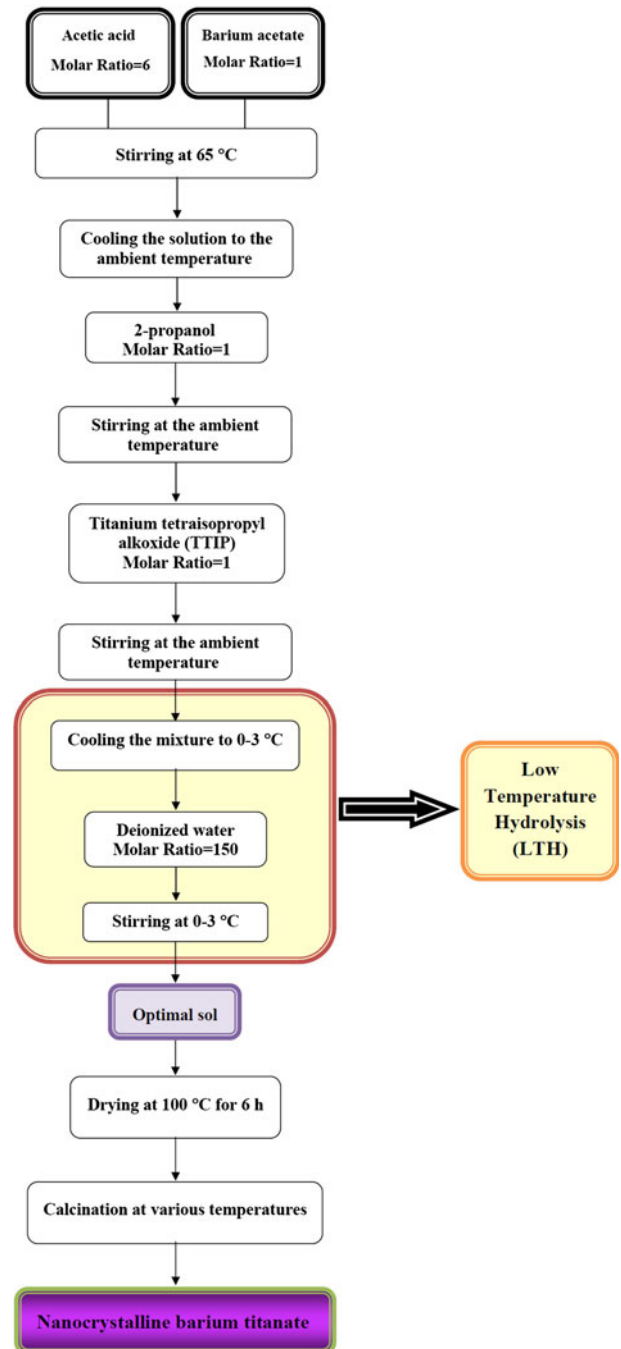

Fig. 1—Flowchart showing the method of preparation of nanocrys-tals and temperature at each step.

B. Sample Characterization

Powder samples are characterized using thermal analysis (DTA/TGA), FTIR, XRD, SEM, and TEM techniques. The differential scanning calorimetric (DSC) measurements and TGA were performed using a thermal analysis system (STA 1500; Rheometric Scientific, Piscataway, NJ), in air, at a heating rate of 5 K (°C)/min, in a platinum crucible with α-Al_2O_3 powder as a reference. Because the samples might slowly react with crucibles, the cooling curves were not measured. Functional groups in xerogel were detected by using of a Hitachi 3140 spectrophotometer FTIR spectroscopy (Hitachi, Tokyo, Japan). IR spectra were recorded in the range of 400 to 4000 cm^{-1} and were measured on samples in KBr pellets. The crystal structure, phases, and average crystallite size of calcined powder were determined by XRD (40 kV, 30 mA, model PW3710; Philips, Amsterdam, the Netherlands) with Cu Kα radiation and scanning speed of 10 deg/min over a range of 5 to 75 deg at room temperature. The morphological features and particle size of the prepared powders were observed using SEM (Vega Tescan XL31; Philips) and TEM (CM200; Philips).

III. RESULTS AND DISCUSSION

A. Modified Method of Preparation of Nanosized Powders

The use of alkoxides as precursors and the sol-gel process for the preparation of metal oxides has been explored with a view to nanostructuring.[12,13] However, the great sensitivity of titanium alkoxides to hydrolysis makes their sol-gel transformation very fast and thus difficult to control. In the proposed method, to control the hydrolysis process and sol-gel transformation, and consequently, to control and modify the process of preparation, more attention was focused on this fact and a two-step hydrolysis process was used. It is found that dilution of titanium alkoxide in a solvent, such as a suitable alcohol, can decrease its reactivity. This fact was used to modify the preparation method as well. In contrast, in the sol-gel method, the processing time and the cost of used materials are the key parameters that we tried to optimize. The results showed that the proposed preparation conditions have a great effect on lowering the synthesis temperature and reducing the synthesis time. The preparation costs are significantly decreased because a much lower amount of 2-propanol and acetic acid was used to prepare of the sol and no modifier was added, such as acetyl acetone. In contrast to other reported data,[14,15] quick preparation is another advantage of the method of preparation because the sol is prepared only in 90 minutes and the required time of xerogels calcination is only 1 hour, which is more desirable from an economical point of view. In addition, in the proposed method, nanostructured powder is prepared at a lower temperature. One of the most important reasons behind this fact is using the LTH process to prepare the samples. LTH can result in fine hydrolysis products. Fine primary products reacted

faster because of their large surface area, and consequently, the reaction of synthesis completed at lower temperature and in a shorter time.

B. DTA/TGA Characterizations

Because of the nature of the process, sol-gel products are amorphous and consequently need subsequent drying and firing treatment to form crystalline products. Sol-gel transformation is a slow process. The two distinct choices to accelerate sol-gel transformation include the use of additives and the use of heat. In the current research, we applied heat to promote sol-gel transformation. Applying heat to sols accelerates the kinetic of agglomeration and gelation, resulting in a shorter sol-gel transformation time (a faster rate in sol-gel transformation). By continuous heating and continuous monitoring of the sample, the events that take place during drying and firing can be inspected and recorded. The main goal of this article is to investigate and monitor the thermally induced changes, events, transformations, and reactions to obtain a better understanding of the synthesis process and mechanism.

For the evaluation of thermal evolutions of xerogel, first, the gels were dried at 373 K (100 °C) for 6 hours, and then as-prepared xerogel was subjected to thermal monitoring through DTA/TGA analysis. Thermal analysis curves were recorded at a temperature range of 323 K to 1473 K (50 °C to 1200 °C) (Figure 2). Thermal decomposition of the dried gel reveals that the total weight loss is approximately 40 pct. Three distinct steps of weight loss were observed in the TGA curve. The first weight loss (approximately 9 pct) observed at approximately 323 K to 512 K (50 °C to 239 °C) is caused by the vaporization of residual or nonstructural water and volatile organic solvents. The second stage of weight loss (approximately 25 pct) observed at approximately 512 K to 843 K (239 °C to 570 °C) is generally attributed to the deformation of gel structure and pyrolysis of the Ba-Ti organic precursors. These processes cause the decomposition of acetate compounds and the vaporization of produced organic compound. The presence of acetate compounds in composition of the gel is caused by the use of acetic acid and barium acetate for the preparation of powder as precursors. Oxidation and the formation of carbonate phases occurred at this step too. This step is accompanied with a weight loss of approximately 25 pct. At this stage of firing, the intermediate
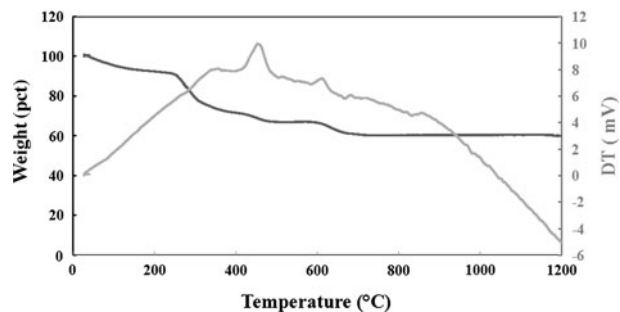

Fig. 2—DTA/TGA curves of the xerogels dried at 373 K (100 °C).

phases (carbonate phases) were formed. This step corresponded to the endothermic peak at 726 K (453 °C) in the DTA curve. The third weight loss observed at approximately 843 K to 1056 K (570 °C to 783 °C) is related to the formation of $BaTiO_3$. Decomposition of barium carbonate release CO_2 and reaction between the resulted barium oxide and TiO_2 led to formation of $BaTiO_3$. This step exhibits a weight loss of approximately 6 pct. This step is correlated with an endothermic peak at 884 K (611 °C) in the DTA curve that directly corresponded to carbonate phase decomposition. No weight loss was observed after this step, which indicates that the formation of barium titanate completes at 1056 K (783 °C). Another exothermic peak, which appears in the DTA curve at 1128 K (855 °C), can be related to the polymorphic transformation (cubic-tetragonal) of barium titanate. In the entire process of thermal decomposition of the xerogel, no weight gain was registered through TGA analysis. These results were used to identify the range of different calcination temperatures. In brief, concluding from the preceding discussions, it can be stated that the main reactions/events occurred with increasing temperature are as follows: (1) dehydration of the polymeric precursors, (2) decomposition/oxidation of the dehydrated polymeric precursor, and (3) formation of barium titanate.

C. *FTIR Characterization*

Chemical bonds vary widely in their sensitivity to probing by infrared techniques. Thus, the potential utility of IR spectrophotometry is a function of the chemical bond of interest, rather than being applicable as a generic probe. In crystalline materials, the many vibrational modes can be classified by the symmetry of their motions and, although they are not rigorous, these assignments can be applied to the glassy material as well. For more quantitative work, the fundamental theory of infrared spectroscopy delineates a band shape analysis. Three characteristics are commonly examined:

peak position, integrated peak intensity, and peak width. Peak position is most commonly exploited for qualitative identification because each chemical functional group displays peaks at a unique set of characteristic frequencies. This provides a fingerprint that can be used to identify chemical groups.[16]

FTIR analysis was carried out at 373 K (100 °C) to detect the presence of functional groups. By using this analysis, the reaction mechanisms in the sol-gel process can be detected. An FTIR analysis of the xerogel is shown in Figure 3. At low temperatures, the IR spectrum is very complex, but at high temperatures, some of the absorption band disappeared and the spectrum became simpler. Consequently, from the fingerprint nature of absorption bands and according to the literature, the characteristic absorption at 3416 cm^{-1} is assigned to the O-H stretching vibration in water and confirms the existence of water in the xerogel.[17] Absorption at 3016 cm^{-1} is caused by C-H stretching vibration and advocates the presence of $-CH_2$ and $-CH_3$ functional groups because of the alkoxide.[18] Two peaks at 1702 cm^{-1} and 1421 cm^{-1} clearly indicates the existence of acetate groups bonded to barium atoms and also advocates the asymmetric [v_{as}(COO-)] and symmetric [v_s(COO-)] stretching vibrations of carboxylate groups.[19] These two absorptions indicate that the acetate ligands are bonded to barium atoms. These absorptions were introduced to spectrum by using the barium acetate as a precursor. When the difference of symmetric and asymmetric absorptions (Δv) is larger than 160 cm^{-1}, the acetate group is a typical bridging bidentate ligand, and when it is smaller than 80 cm^{-1}, it is a chelating bidentate ligand.[20] In the current case, this group is a bridging ligand. The characteristic absorption at 1567 cm^{-1} is assigned to the O-H stretching vibration in alcohol and confirms the existence of alcohol in the xerogel.[4] This absorption is different from the previous O-H stretching vibration that was related to water. The absorption bands at 1331, 1049, 1022, and 934 cm^{-1} can be considered as the alcoholic bending vibrations. Finally, absorption bands at wave
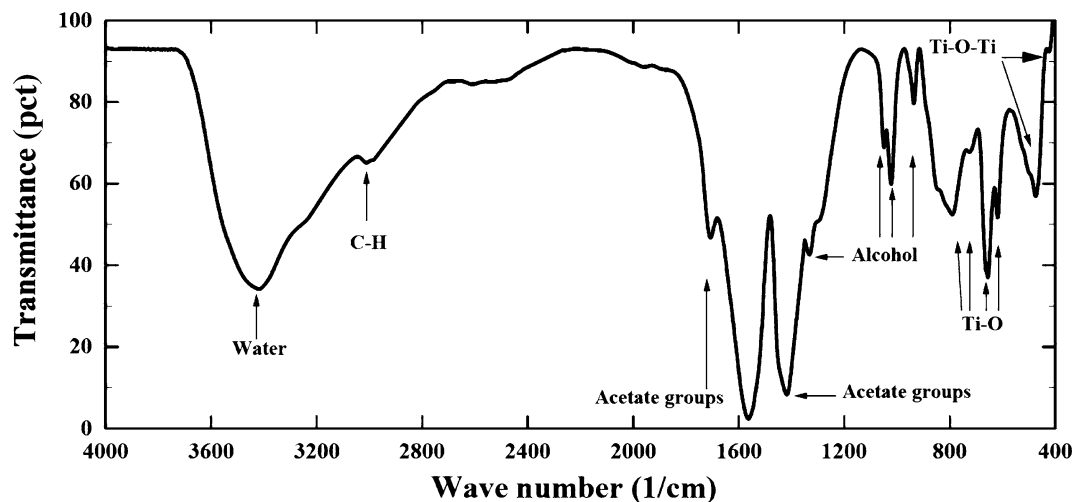

Fig. 3—The FTIR spectrum of the xerogels dried at 373 K (100 °C).

Table I. Origin of Relevant Infrared Absorption Frequencies of the Xerogels Dried at 373 K (100 °C)

| Sample Description	Peak Position (cm^{-1})	Mode of Vibration	Originated From	Ref.
Xerogel (dried gel)	3416	O-H stretching vibration in water	presence of water in the xerogel	[17]
	3016	C-H stretching vibration mode	presence of –CH_2 and –CH_3 functional groups that are caused by the alkoxide	[18]
	1702	asymmetric [v_{as}(COO-)] stretching vibrations of carboxylate groups	presence of acetate groups bonded to barium atoms	[19]
	1567	O-H stretching vibration in alcohol	presence of alcohol (2_propanol) in the xerogel	[4]
	1421	symmetric [v_s(COO-)] stretching vibrations of carboxylate groups	presence of acetate groups bonded to barium atoms	[19]
	1331, 1049, 1022, and 934	C-H bending vibration mode	presence of alcohol (2_propanol) in the xerogel	[21]
	wave numbers greater than 800	Ti-O vibration modes	Ti-O and Ti-O-Ti vibrations	[21]
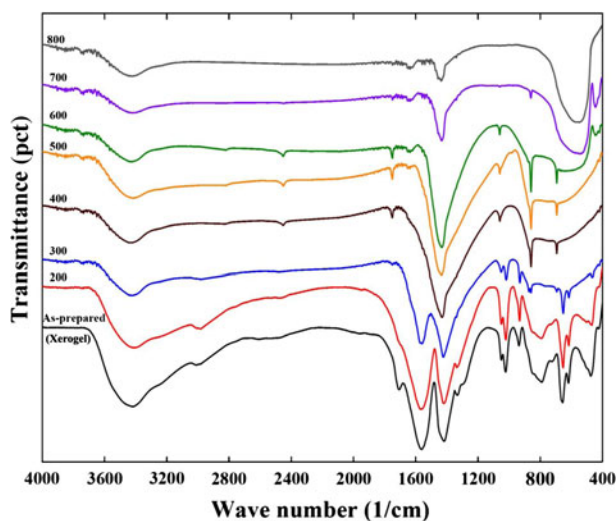
Fig. 4—The FTIR spectra of the xerogel at different temperatures.

numbers greater than 800 cm^{-1} are related to M-O bands,[21] which result from the Ti-O and Ti-O-Ti bands.[22,23] The preceding results are also briefly summarized in the Table I.

The Beer-Lambert law is a simplification of the analysis of the second band shape characteristic: the integrated peak intensity. If a band arises from a particular vibrational mode, then to the first order, the integrated intensity is proportional to the concentration of absorbing bonds.[16] The intensity of peaks in the xerogel spectrum is rather high compared with the spectra at higher temperatures. On the one hand, this fact indicates that the concentration of corresponding absorbing bonds is high in the xerogel. On the other hand, this fact may be an indication of amorphous structure of xerogel.

Figure 4 shows the FTIR spectra of the xerogel at different temperatures. It is known that the absorption band width—the third characteristic of a band—which is usually expressed as the full width at half maximum (FWHM) is a function of the homogeneity of the chemical bonding. Small variations in bond strengths cause small shifts in peak positions resulting in broadening of the absorption band. The effect of curing a material can be observed by a peak-width analysis. As one anneals the defects, the bands become narrower and more intense (to conserve area, if no bonds are created or destroyed).[16] In general, in contrast to xerogel spectrum, three events occurred in the current spectra:

(i) Disappearance some absorption bands: The removal of the volatile materials such as alcohol and at a higher temperature might be caused by crystallizing the amorphous structure of the sample.
(ii) Increase in absorption bands intensity and decrease in its width: If no bonds are created or destroyed, then the absorption band intensity is proportional to the concentration of the absorbing bonds, possibly because of an increase in the homogeneity of the current chemical bonds.
(iii) Appearance some new absorption bands: New absorption bands frequently appeared at higher temperatures because of new functional groups. The nature of materials changed because of chemical reactions that occurred at a higher temperature possibly because of recrystallization of the sample.

In an analysis of the spectra, it can be stated that broad bands at 3416 cm^{-1} are attributed to O–H stretching vibration. The intensity of this band tended to decrease with increasing calcination temperature, but this band persisted up to 1073 K (800 °C). The decrease of intensity at lower temperatures is caused by removing water from the xerogel, and its persistence at higher temperature is caused by the absorption of moisture during the standard method of preparation of samples (powders of KBr and powder of sample were blended together to make the sample, and by using water and pressing, the pallet was prepared for the spectroscopy evaluation). It is revealed that after firing at 473 K (200 °C), the intensity of characteristic absorption bands of water (at 3416 cm^{-1}), alkoxide (at 3016 cm^{-1}), and alcohol (1331 cm^{-1}) decreased in contrast to the xerogel spectrum, and one of the characteristic absorptions of the acetate (1702 cm^{-1})

disappeared. These facts are evidence of removing these volatile organic solvents progressively. In this condition, no significant change was observed in the intensity of other absorption bands. The sharper decrease in intensity of the mentioned bands and the some other absorption bands including water, alkoxide, acetate, and alcohol was observed between 473 K and 673 K (200 °C and 400 °C). In the mentioned temperature range, some bands disappeared that indicates the removing corresponding volatile organic solvents. After firing at 673 K (400 °C), the characteristic absorptions of alkoxide, alcohol, and acetate groups disappeared, and new bands at 2454, 1750, and 693 cm^{-1} appeared in the spectrum. These three absorptions are evidence of carbonation at 673 K (400 °C) in air. These absorptions originated from thermal pyrolysis of acetate groups bonded to barium.[4] FTIR is among the most sensitive techniques to detect traces of $BaCO_3$ in quantities as small as 0.6 wt pct.[24] The thermal pyrolysis reaction of acetate completes gradually as follows:

$$Ba(CH_3COO)_2 + 4O_2 + \rightarrow BaCO_3 + 3H_2O + 3CO_2 \quad [1]$$
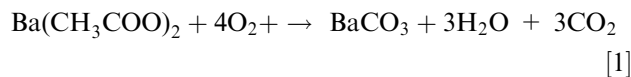
It is obvious that oxygen atmosphere facilitates this reaction. It is evident that this reaction is accompanied by weight loss. According to the TGA results, maximum weight loss occurs during this reaction. The appearance of absorption band at 1057 cm^{-1} at 673 K (400 °C) can be assigned to carboxylate groups bonded to titanium. This peak disappears at higher temperature (973 K [700 °C]) because of its decomposition. At 673 K (400 °C), the Ti-O characteristic bands disappeared and an absorption at 850 cm^{-1} appeared as a result of TiO_2.[24] The intensity of this absorption band increases up to 873 K (600 °C). At higher temperatures, an inverse behavior was observed, and at 1073 K (800 °C) Ti-O characteristic bands were completely disappeared. After firing at 773 K (500 °C), the intensity of characteristic absorption bands of carbonates increases, indicating an increase in carbonates concentration. At a higher temperature, the intensity of carbonate bands (2454, 1750, and 693 cm^{-1}) gradually decreased up to 973 K (700 °C), indicating the decomposition of carbonate phase. These two facts indicate that the maximum rate of carbonation and maximum concentration of carbonates is at a temperature of approximately 773 K (500 °C). At 873 K (600 °C), an absorption band appeared at 440 cm^{-1} as a result of TiO_2.[25] The intensity of this band at 973 K (700 °C) increased, and this band disappeared from the spectrum at 1073 K (800 °C) because of barium titanate formation. The decomposition of carbonates occurs according the following reaction:

$$BaCO_3 \rightarrow BaO + CO_2 \quad [2]$$
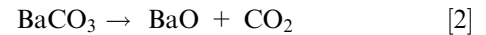
After this reaction, CO_2 released from the sample, which corresponds to the third step of TGA (i.e., endothermic peak at 884 K [611 °C] in the DTA curve). The reaction of resulted barium oxide with titanium oxide leads to barium titanate formation. This reaction can occur and initiate after barium carbonate decomposition, but at higher temperatures, the rate of reaction increases. The reaction of barium titanate formation is as follows:

$$BaO + TiO_2 \rightarrow BaTiO_3 \quad [3]$$

At 973 K (700 °C), another absorption band appeared at 1628 cm^{-1} and persisted up to 1073 K (800 °C). This absorption band is caused by the presence of adsorbed moisture.[26] At 973 K (700 °C), an absorption band appeared in the spectrum at 539 cm^{-1}, which was assigned to barium titanate formation,[26] and at a higher temperature, its intensity increased, confirming the increase of barium titanate formation. At 973 K (700 °C), carbonate and Ti-O absorption bands disappear and the intensity of absorption bands at 1057 and 850 decreased. Consequently, barium titanate was formed according the previous reaction. The infrared spectrum of the sample calcined at 1073 K (800 °C) is close to the standard spectrum of the $BaTiO_3$. At this temperature, there are four absorption bands at 3416, 1628, 1432, and 539 cm^{-1}. The absorption bands at 3416 and 1628 cm^{-1} are caused by the presence of adsorbed moisture, and the absorption bands at 1432 and 539 cm^{-1} are caused by $BaTiO_3$.[26] The results also indicated that the barium titanate preparation was completed at 1073 K (800 °C). In Table II, the most important thermally induced events and the corresponding temperatures are summarized.

D. XRD Characterization (Effect of Calcination Temperature)

In mass production, reduction of the process time can lead to an increase in the rate of production. Sol-gel

Table II. The Most Important Thermally Induced Events Indicated by FTIR

Temperature [K (°C)]	Thermally Induced Events
373 (100)	xerogel formation
473 (200)	initiation of removing of water, alkoxide, acetate, and alcohol
573 (300)	sharper decrease in amount of water, alkoxide, acetate, and alcohol
673 (400)	pyrolysis of acetate groups and formation of carbonates
773 (500)	sharper increase in concentration of carbonates
873 (600)	initiation of decomposition of carbonates and initiation of the formation of $BaTiO_3$
973 (700)	sharper increase in concentration of $BaTiO_3$ and sharper decrease in concentration of carbonates
1073 (800)	preparation of pure barium titanate nanoscale powder

transformation can be accelerated by a change in its equilibrium conditions such as increasing the temperature. During a polycondensation reaction (gelation), the molecules bonds with each other to create a polymeric macrostructure or macromolecule. This process needs enough time to complete. The increase in temperature can dramatically accelerate the polycondensation process, which has endothermic nature, and as a result, the sol transforms into a gel in a very short time. A very small fraction of the total weight of a gel is related to the final product. A significant fraction of the total weight of a gel is related to water and the other volatile organic materials, which are removed gradually in the drying and firing stages depending on their bond strengths. Because of the use of barium acetate, acetic acid, and 2_propanol as precursors, it is expected to detect carbonate phases formation during firing process. As a result of the nature of sol-gel process and its related reactions, the sol-gel products are amorphous; therefore, they need subsequent drying and calcinations to form crystalline products.

The XRD method is a powerful nondestructive tool that can provide information with regard to crystal structure, plane of orientation, strain relaxation, *etc.* Powder samples were calcined for 1 hour in air at different temperatures and cooled in the furnace. Figure 5 shows the XRD patterns measured at room temperature of the calcined powders at different temperatures. XRD is not informative about the amorphous materials because the patterns of these materials do not

have any characteristic peak. Consequently, we did not prepare the XRD pattern of the xerogel. The gels dried at temperatures below 573 K (300 °C) were found to be amorphous and have not been indicated in the current figure. FTIR spectroscopy is a better candidate for the analysis of amorphous materials. Contrary to other established methods,[19,27,28] at all temperatures, we did not detect any intermediate phases like $Ba_2Ti_2O_5CO_3$ or Ba2TiO$_4$. This fact can be used for preparing high-purity barium titanate. This fact has a vital role for several applications of barium titanate-like capacitors. By introducing impurities into an insulator, the insulating behavior can be changed into a semiconducting nature. Purity is also a key required property in other advanced application of barium titanate. A weak trace ($2\theta = 26.47$ deg) of TiO_2 (anatase phase) resulting from hydrolysis reactions was detected in the powder calcinated at 573 K (300 °C). When the temperature increased up to 573 K (300 °C), $Ti(OH)_4$, which is the product of hydrolysis reaction, decomposed according to the following reaction, and consequently, the anatase TiO_2 phase was formed:

$$Ti(OH)_4 \rightarrow TiO_2 + 2H_2O \qquad [4]$$
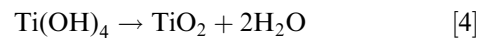
At 673 K (400 °C), the structure deformation of gel occurred, and by decomposition of acetate compounds, the carbonate phase begins to crystallize according to Reaction [1]. With increasing the temperature up to 873 K (600 °C), the number and intensity of peaks corresponding to the barium carbonate phase increased. At this temperature for the first time, barium titanate peaks appeared in the pattern. The appearance of X-ray reflections at 2θ, such as 31.49, 38.79, 45.23, 50.79, and 65.85, supports the formation of barium titanate. The XRD pattern indicates the presence of cubic $BaTiO_3$ phase (with an average crystallite size of 6 nm) and barium carbonate (JCPDS Table no. 45-1471) at 873 K (600 °C). At 973 K (700 °C), by subsequent decomposition of barium carbonate, the amount of barium carbonate decreases. At this temperature, the XRD pattern indicates the presence of dominant cubic phase of $BaTiO_3$ with an average crystallite size of 19 nm and with little trace of barium carbonate. When the samples were fired at 1073 K (800 °C), the trace of barium carbonate disappeared and the pattern shows a fully crystallized cubic perovskite structure (JCPDS Table no. 31-174) with an average crystallite size of 25.9 nm. The barium titanate nanopowders were characterized by well-resolved peaks at 22.15, 31.49, 38.79, 45.23, 50.79, 56.09, 65.85, and 70.17 corresponding to the (1 0 0), (1 1 0), (1 1 1), (2 0 0), (2 1 0), (2 1 1), (2 2 0), and (2 1 2) planes. The second peak observed at $2\theta = 31.49$ deg matches the highest intensity peak of $BaTiO_3$, corresponding to the (1 1 0) plane of the barium titanate perovskite structure, confirming that the particles are preferably orientated along (1 1 0) plane. By increasing the temperature until 1173 K (900 °C), the intensity of the peaks increased. Moreover, at 1173 K (900 °C), the FWHM intensity decreased, and consequently, the average crystallite size increased from 25.9 to 31.8 nm.
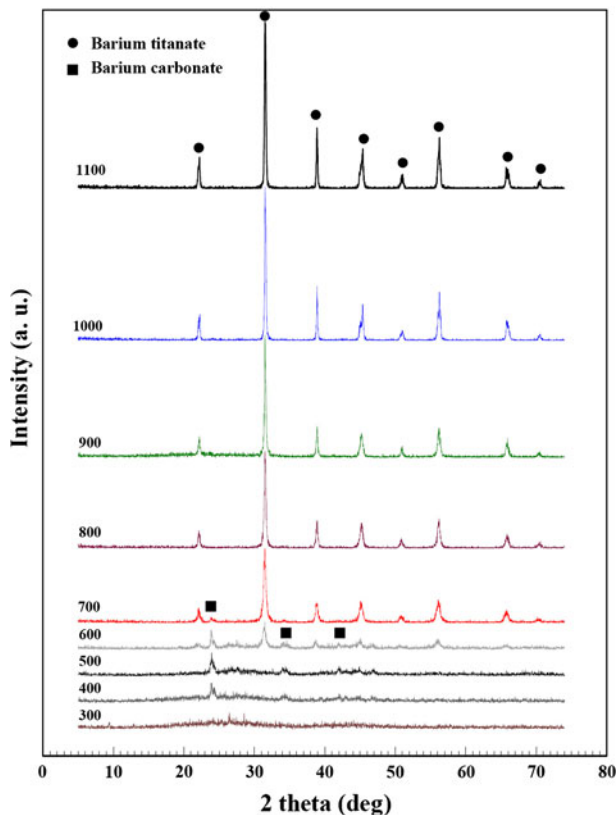

Fig. 5—XRD patterns of powders calcined at different temperatures for 1 h.

In the current research, tetragonal barium titanate nanoparticles (JCPDS Table no. 5-0626) were synthesized at a lower temperature. One difficulty in quantification of the tetragonality of barium titanate is the interpretation of the XRD measurement of (2 0 0) and (0 0 2) peaks. Theoretically, 100 pct tetragonal barium titanate has two separate peaks between $2\theta = 44$ deg and 47 deg (Figure 6). Complete cubic barium titanate shows just one peak. A mixture of tetragonal and cubic barium titanate will show all intermediate forms between one and two peaks. When the xerogel was fired at 1173 K (900 °C) for 1 hour, peak splitting occurred at approximately $2\theta = 45.3$ deg (Figure 7), which is a result of the tetragonal phase. This fact was also clearly indicated by DTA results. When the xerogels were fired at higher temperatures (1273 K and 1373 K [1000 °C and 1100 °C]), the amount of splitting of the mentioned peak increased. All XRD patterns at temperature range of 1173 K to 1373 K (900 °C to 1100 °C) match well with tetragonal barium titanate, exhibiting a peak split between 2θ from 44.77 deg to 45.38 deg. The width of split refers to the amount of progress in the cubic to tetragonal transformation. The tetragonality of the barium titanate powder was increased with an increase in the calcination temperature.

Table III shows quantitative XRD phase analysis, including the amount of existing crystalline phases, their crystallite size, and the tetragonality measurement. The relative amounts of the perovskite phase were calculated by measuring the major peak intensities of the perovskite phase and barium carbonate. The percentage of perovskite was estimated by the following equation:

$$\text{pct perovskite} = \left(\frac{I_{\text{perovskite}}}{I_{\text{perovskite}} + I_{\text{barium carbonate}}} \right) \times 100$$

[5]

where $I_{\text{perovskite}}$ and $I_{\text{barium carbonate}}$ refer to the intensity of the (1 1 0) perovskite peak and the intensity of the highest intensity $BaCO_3$ peak, respectively. This equation is well known and widely employed in connection with the preparation of complex perovskite structure materials.[30] It is important to note that the reported data were calculated based on the crystalline phases only. At 573 K and 673 K (300 °C and 400 °C), the samples consist of a mixture of amorphous and crystalline phases. The percentage of the perovskite phase was increased with increasing calcination temperatures. The average crystallite size of barium carbonate and $BaTiO_3$ at different temperatures calculated using Scherrer's formula[31]:

$$D = \frac{0.9\lambda}{\beta \cos \theta}$$

[6]

where D is the average crystallite size, $\lambda = 1.541$ Å (X-ray wavelength), and β is the width of the diffraction peak at half maximum for the diffraction angle 2θ. The average crystallite size of $BaTiO_3$ was calculated from (1 1 0) peak of the corresponding XRD pattern, and the
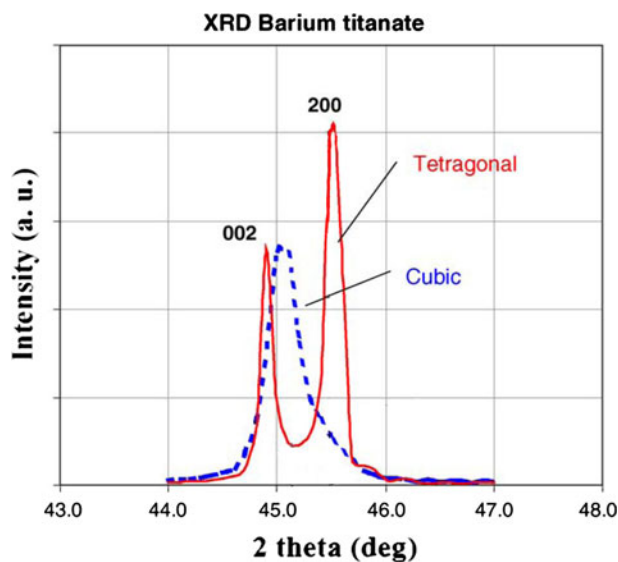

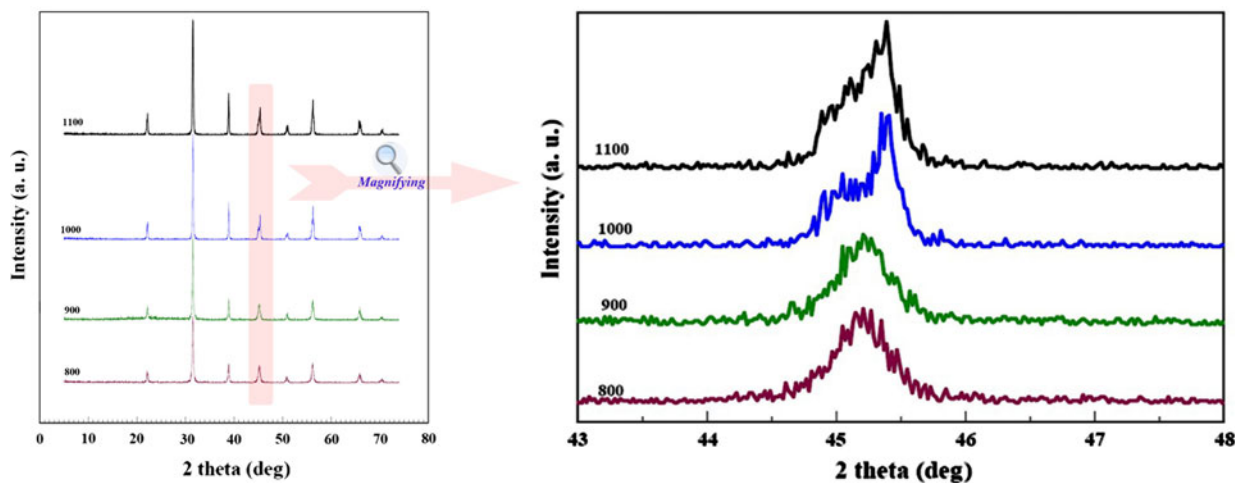Fig. 6—Example of XRD curves cubic and tetragonal barium titanate: reproduced after Ref. 29.

Fig. 7—XRD observation on the (200) peak broadening at 45.3 deg of samples at different calcination temperatures.

Table III. The Phase Evolution and Quantification, Crystallite Size, and Tetragonality Evaluation with Respect to Calcination Temperature

| Calcination Temperature [K (°C)] | Main Phase | Minor Phase | Crystalline Phase* (pct) | | Average Crystallite Size | | Tetragonality (c/a) |
			Carbonate Phase	Perovskite Phase	Barium Carbonate	Barium Titanate	
573 (300)	amorphous phase	anatase	0	0	—	—	—
673 (400)	amorphous phase	barium carbonate	100	0	31.9	—	—
773 (500)	barium carbonate	barium titanate	83	17	56.7	—	—
873 (600)	barium titanate	barium carbonate	41.6	58.4	70.8	6	—
973 (700)	barium titanate	barium carbonate	4.8	95.2	29	19.5	—
1073 (800)	barium titanate	—	0	100	—	25.9	—
1173 (900)	barium titanate	—	0	100	—	31.8	1.00278
1273 (1000)	barium titanate	—	0	100	—	40.1	1.00609
1373 (1100)	barium titanate	—	0	100	—	44.6	1.01067

*The volume fractions are calculated based on the current crystalline phase. The amorphous phases are ignored when calculating the volume fraction of crystalline phase.

results are presented Table III. The results illustrated that the crystallites are nanometric sized, and the average crystallite size of barium carbonate and barium titanate were increased with increasing calcination temperature. With increasing calcination temperature from 873 K to 1373 K (600 °C to 1100 °C), the average crystallite size was increased from 6 to 44.6 nm. At temperatures above 1073 K (800 °C), the thermal energy of calcination is spent to make progress in the polymorphic transformation and simultaneously for the growth of crystallites. This fact decreases the growth rate in contrast to the sample calcined at lower temperatures. The tetragonality (c/a), calculated through the indexes of XRD patterns, of barium titanate nanopowders at different calcination temperatures is shown in Table III. At temperatures lower than 1073 K (800 °C), the powder did not exhibit tetragonal structure. The tetragonality of powders tended to increase with increasing calcination temperatures, and at 1373 K (1100 °C), the tetragonality of sample is close to a fully tetragonal value of 1.01.

E. The Advantages of the Preparation Method

The significant advantage of this method is the synthesis of finer nanocrystals at a lower temperature and in a shorter period of time. For example, Tangwiwat and Milne[19] could not prepare the pure barium titanate even at 1173 K (900 °C), and at this temperature, traces of byproducts were detected in the prepared powder. Xing et al.,[14] Yu and Cui,[32] Lee and Zhang[15] synthesized pure cubic BaTiO$_3$ by calcination at 1073 K (800 °C) for 4 hours, 1173 K (900 °C) for 2 hours, and 1073 K (800 °C) for 2 hours, respectively, but in the current research, pure cubic BaTiO$_3$ was prepared after calcination at 1073 K (800 °C) for 1 hour. At 973 K (700 °C), only a weak trace of barium carbonate phase was detected. It can be concluded that the smaller amounts of 2-propanol and acetic acid can result in reducing the formation of carbonate phases during the calcination process. This fact results in a reduction of the required time and temperature for

calcination and synthesis. Moreover, in the current research, no modifier such as acetyl acetone has been used. The modifier can affect the time and temperature of calcination. After decomposition of barium carbonate and its reaction with TiO$_2$, BaTiO$_3$ formed according to Reactions [2] and [3]. BaTiO$_3$ formation can be obtained through (1) the interfacial reaction between BaCO$_3$ and TiO$_2$ and then (2) the diffusion of Ba^{+2} ions along the surfaces or grain boundaries of BaTiO$_3$ nanoparticles. According to the considered reaction pattern, the formation of BaTiO$_3$ in the initial stage of the reaction between BaCO$_3$ and TiO$_2$ depends on the BaCO$_3$ decomposition. From the thermodynamics point of view, this reaction has the potential capability of happening, and from the kinetics point of view, it needs enough energy to climb the activation energy barrier and initiate the reaction. This energy can be provided by the calcination process. However, with an increase in the amount of carbonate phases, their decomposition needs more energy and a longer time of calcination. As a consequence, BaTiO$_3$ formation will occur at higher temperature and for longer times. In the second stage, the barium titanate formation is controlled by the barium diffusion through barium titanate layer. Usually, in this stage, secondary phases are formed. But in the current research, a fine structure of the nanopowders is an effective way of limiting and preventing the formation of secondary phases. The size-dependent effects of nanoparticles reduce the dependence of their purity on diffusion mechanism. The preparation of finer nanocrystals is another advantage of the proposed preparation method. The following is example of evidence that supports the previously mentioned claim. In the similar research,[15] prepared powders had crystallite size in the range of 30 to 60 nm at temperature between 1073 K and 1273 K (800 °C and 1000 °C), but under the same conditions, our results were in range of 25 to 40 nm. Moreover, in the current research, tetragonal barium titanate nanoparticles were synthesized at a lower temperature. This fact is one of the most important advantages of our modified method. For example, the synthesis routes proposed by Xing et al.,[14]
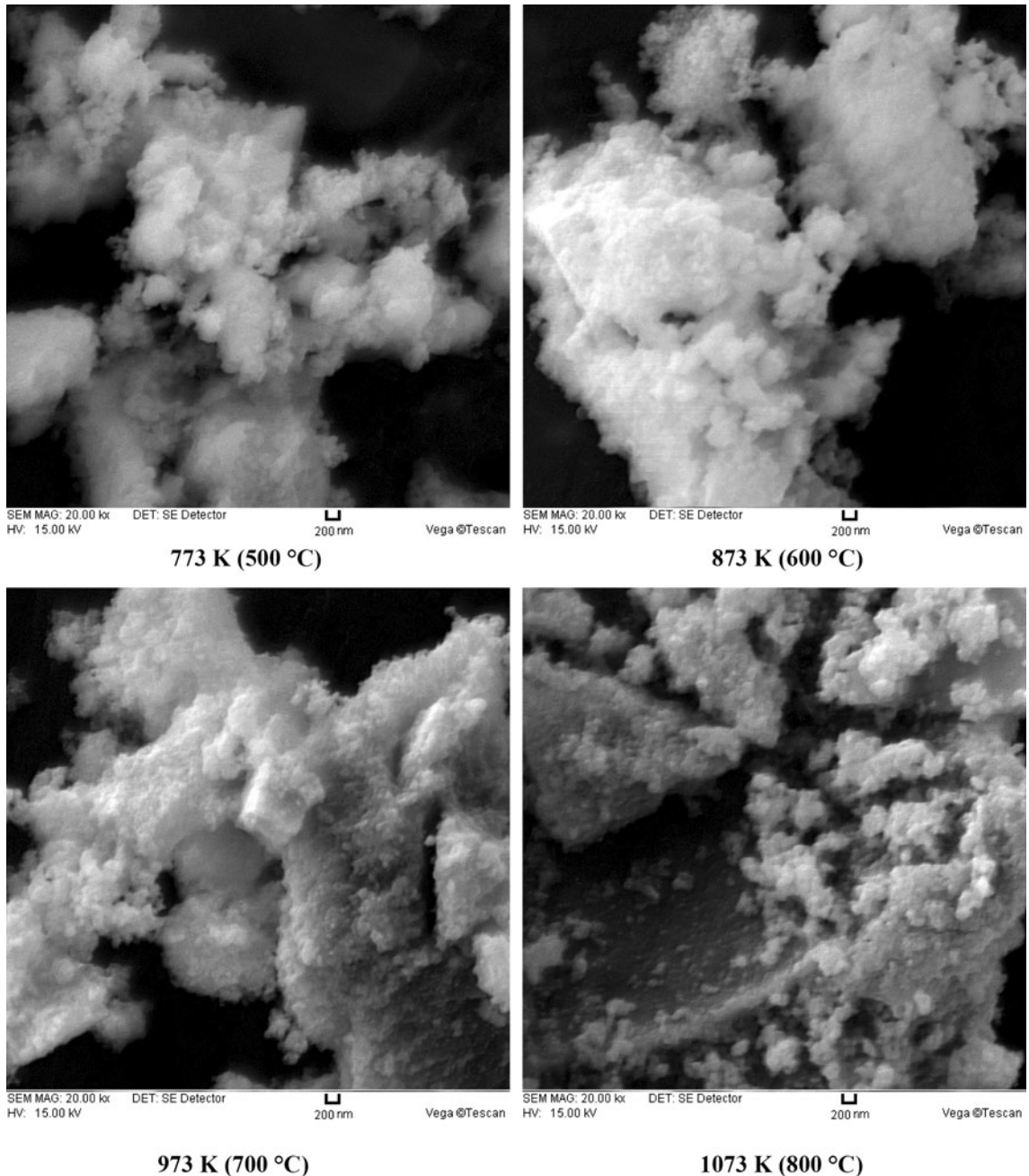
773 K (500 °C)

873 K (600 °C)

973 K (700 °C)

1073 K (800 °C)

Fig. 8—SEM images of powders calcined at different temperatures for 1 h.

Harizanov[11] were successful in producing tetragonal BaTiO$_3$ after calcination at 1173 K (900 °C) for 2 hours and 1273 K (1000 °C) for 1 hour, respectively. Moreover, Lee and Zhang[15] could not prepare tetragonal barium titanate even after firing to 1273 K (1100 °C).

In this work, the previously mentioned advantages were achieved by making modifications to the process of preparation of the nanopowders. According to this point of view, we modified our method by choosing appropriate precursors, using optimized precursor's ratios and manipulating the process of preparation by using the LTH process to prepare fine and pure barium titanate at a lower temperature and a shorter period of time.

F. Electron Microscopy Characterization (SEM and TEM)

The SEM is often the first analytical instrument used when a "quick look" at a material is required and the light microscope no longer provides adequate resolution. SEM micrographs of BaTiO$_3$ powders calcined at different temperatures (773 K to 1073 K [500 °C to 800 °C]) showing morphology and particle size of products are illustrated in Figure 8. All the powders obviously seem to be highly agglomerated primarily because of the various processes and reactions that occur during drying of the gel precursor. A TEM micrograph confirms that the powders are highly

agglomerated. Figure 9 shows the TEM micrograph of the powder obtained by calcining for 1 hour at 1073 K (800 °C). This micrograph shows BaTiO$_3$ nanoparticles and some nanometric agglomerates. However, the crystallite size of particles was in the range of 6 to 53 nm and the average crystallite size is approximately 29 nm, which is in good agreement with the data obtained from the Scherrer equation (Table III). The selected-area electron diffraction (SAED) pattern exhibits hazy circles at the center, which indicates the powders are nanocrystalline. This pattern also shows the presence of concentric rings that confirms the polycrystallinity of the agglomerates.

It is apparent that the nanoscale barium titanate products are homogeneous and compact. All the SEM micrographs exhibited particles greater than the average crystallite size determined by the analysis of XRD (Table III), suggesting an internal structure of the agglomerated particles. Moreover, small particles embedded in each agglomerated cluster correspond to the barium carbonate and barium titanate crystallites with respect to their calcination temperature. The morphological properties and size distribution characterization of the prepared powders indicate that the products consist of somewhat regularly shaped and relatively spherical particles with a relatively narrow size distribution at various temperatures. Comparatively, the particles calcined at higher temperatures had bigger and harder agglomerates and had particles with more regular and homogenous shape. In these conditions, the particles were more uniform sized and were mostly spherical. An SEM observation indicates that the prepared barium titanate powders at 773 K and 873 K (500 °C and 600 °C) were not so well crystallized. In these conditions, the particle size distribution of the samples was broader in contrast to samples calcined at higher temperatures because both the amorphous and crystalline phases were present at these temperatures. In contrast, nucleation of crystallites preferentially occurs at lower temperatures (in the samples calcined at 773 K

Fig. 9—TEM micrograph showing BaTiO$_3$ powders synthesized at 1073 K (800 °C) for 1 h and SAED pattern (inset) of BaTiO$_3$ powders.

and 873 K [500 °C and 600 °C] and were not well crystallized) and crystallite growth occurs at higher temperatures (at 973 K and 1073 K [700 °C and 800 °C] and above). According the SEM micrographs, it can be stated that with increasing calcination temperature, the width of the particle size distribution becomes narrower. It should be noted that the atomic diffusion is required for initiating the particle growth. In a diffusion-type process, the temperature is much more effective than time on the rate of the process, which is a result of the exponential relationship between the rate of growth process and the temperature. At higher temperatures, the particles grow together and the particle size distribution becomes narrower. In contrast, at higher calcination temperatures, especially at 1073 K (800 °C), the absorbed thermal energy was absolutely used to grow the crystallites and particles. Nevertheless, at lower calcination temperatures, the absorbed thermal energy was used to make progress of the nucleation and growth processes. This fact causes nucleation of new generations of particles and simultaneous growth of nucleated particles. Consequently, particle size distribution tends to broaden at lower calcination temperatures. According to XRD results (Table III), the crystallites and particles that exist in the sample calcined at 773 K (500 °C) are assigned to barium carbonate. In the other samples, the crystallite size and particles size tended to increase with increasing calcination temperatures with the exception of the sample that calcined at 973 K (700 °C). This fact will be discussed subsequently. According to Table III (especially concerning the volume fraction of crystalline phase and the crystallite size data), it can be stated that the particles that exist in the SEM micrograph of sample calcined at temperature 873 K (600 °C) may be assigned to the barium carbonate. At 973 K (700 °C), the dominant phase was barium titanate, but the particle size of barium carbonate was larger. In contrast, energy-dispersive X-ray spectroscopy (analysis) cannot help us regarding this challenge (to identify the nature of particles) because the spot size for this analysis was 1 μm (in diameter), which is larger than average particle size. Therefore, we cannot certainly identify the nature of the particles. Although at temperatures below 1073 K (800 °C) we cannot certainly determine the nature of particles, it is obvious that all the samples at all the temperatures are nanostructured. Comparing the SEM micrographs of samples calcined at 873 K (600 °C) with 973 K (700 °C), it can be stated that the first sample exhibited larger particle size than the second one, which is contrary to the general expectation. This fact is caused by phase evolution of barium carbonate according to Reactions [2] and [3]. These reactions are reconstruction-type transformations and consequently are diffusion-control reactions. These types of reaction and phase transformation require nucleation and growth. The faster nucleation rate of barium titanate at 973 K (700 °C) results in a decrease of particle size at this temperature compared with the sample calcined at 873 K (600 °C). This fact was previously indicated by the XRD results (the average crystallite size of the samples that was shown in Table III).
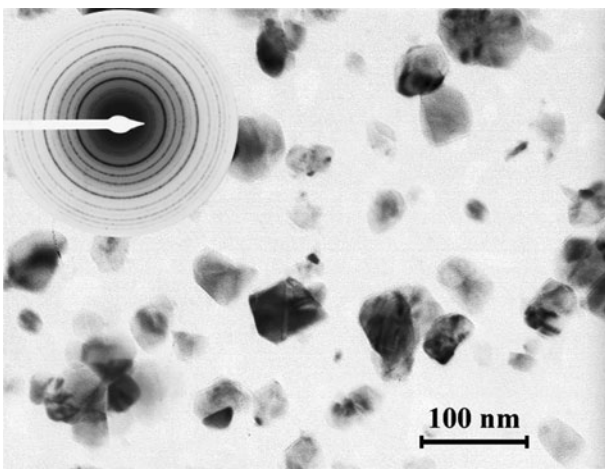
G. *Effect of Calcination Time*

XRD characterization was applied on samples at 1073 K (800 °C) to evaluate the effect of calcination time (Figure 10). The average crystallite sizes of $BaTiO_3$ nanopowders were presented in Figure 11. With an increase in calcination time, the intensity of peaks increased but the width of the peaks decreased because of the growth of the crystallites of the barium titanate. The average crystallite size increased from 23.7 to 36.1 nm with an increase of calcination time from 0.5 to 4 hours. Enough time and temperature is required for the growth process because of its diffusion-type nature. When the calcination time increases, the crystallites have more time to grow. This fact results in decrease of the FWHM and an increase of the intensity of XRD peaks. Figure 10 indicated that the increase of calcination time from 0.5 to 4 hours did not cause the polymorphic transformation. In this regard, it can be said that the calcination temperature increase has a more pronounced effect on the progress of polymorphic transformation compared with the calcination time. The absence of tetragonal phase in samples calcined at 1073 K (800 °C) for 4 hours indicates that polymorphism transformation needs more energy and a higher calcination temperature to occur.

SEM micrographs of powders calcined at 1073 K (800 °C) for 1 and 4 hours are illustrated in Figure 12. The sample calcined for 4 hours exhibited somewhat larger particles with a narrower size distribution in contrast to the other samples because of the growth of the crystallites that was previously indicated by XRD
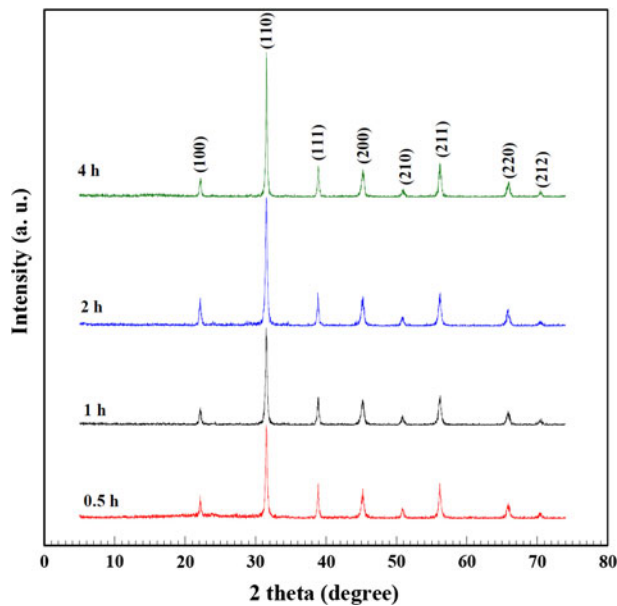

1 h

Fig. 10—XRD patterns of powders calcined at 1073 K (800 °C) with different calcination time.
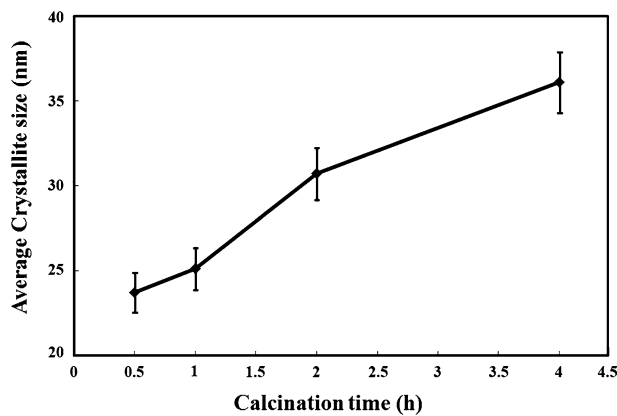
Fig. 11—Effect of calcination time on crystallite size of powders prepared at 1073 K (800 °C).
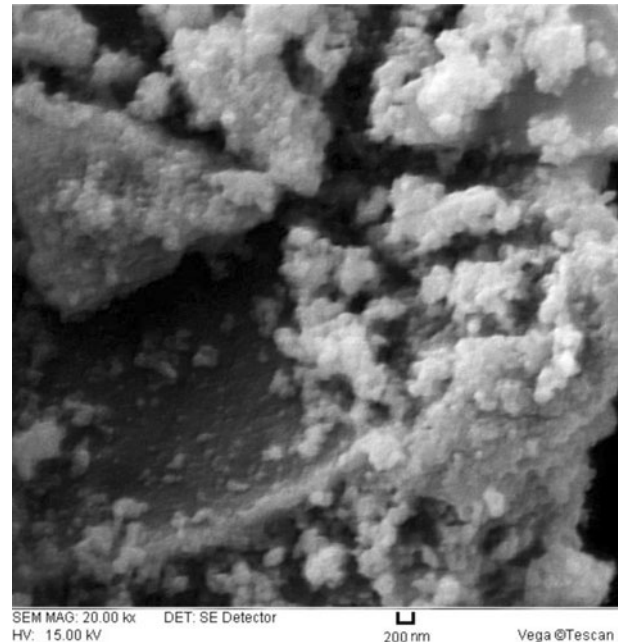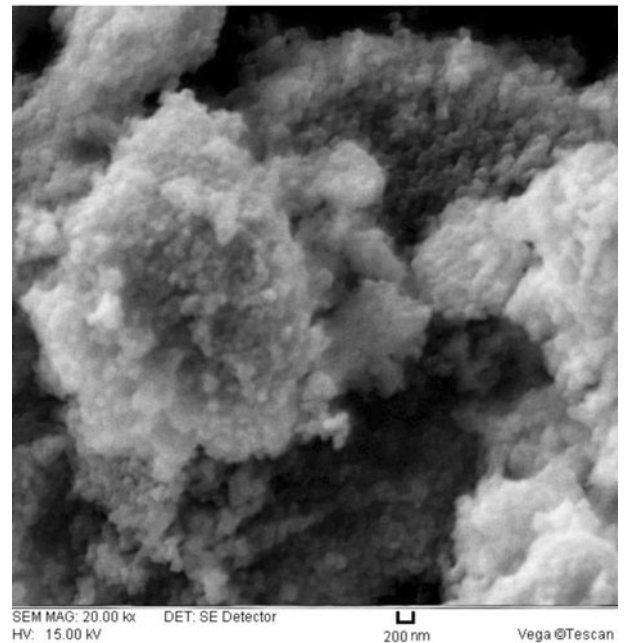
4 h

Fig. 12—SEM images of powders calcined at 1073 K (800 °C) for 1 h and 4 h.

results (Figures 10 and 11). A comparison between these two micrographs and the micrographs of samples calcined at 773 K, 873 K, and 973 K (500 °C, 600 °C, and 700 °C) indicated that particle size was more sensitive to calcination temperature than calcination time because growth is a diffusion-controlled process.

At the end, it can be stated that the sol-gel process is a good approach for nanomaterials synthesis,[33] and consequently, it is a good approach to meet the $BaTiO_3$ ferroelectric memories, nanoelectronic devices, and MLCC trends toward miniaturization and simultaneously high performance.

IV. CONCLUSIONS

In the current research, a modified method with a high degree of reproducibility was proposed for the preparation of fine nanoscale and high-purity $BaTiO_3$ at lower temperature and in shorter time span. A detailed analysis was carried out for the characterization of nanoscale $BaTiO_3$ particles *via* DTA/TGA, FTIR, XRD, SEM, and TEM techniques aided by theoretical calculations. Generally, the results of each characterization method were supported by the others. Pure and single-phase $BaTiO_3$ nanopowders were prepared after 1 hour calcination of polymeric precursor in air at low synthesis temperature (1073 K [800 °C]). The detailed chemical mechanism and reaction patterns of the preparation process were determined by using a combination of different characterization methods. According to the considered reaction pattern, the formation of $BaTiO_3$ in the initial stage of the reaction between $BaCO_3$ and TiO_2 depends on the $BaCO_3$ decomposition. In the second stage, the $BaTiO_3$ formation is controlled by the barium diffusion through barium titanate layer. In this stage, in contrast to the literature, no secondary phase was detected. The crystallite size of $BaTiO_3$ and its tetragonality tended to increase with increasing calcination temperatures. The overall characterization showed in the process of preparation the temperature is more effective than time on the progress because of its diffusion-controlled nature. All the described advantages and excellences of proposed method in contrast to literature seem to be caused by a modified method and its optimizations. The overall evaluation indicated that the current method of preparation is a cost-effective method and is a good candidate for mass production.

REFERENCES

1. S. O'Brien, L. Brus, and C.B. Murray: *J. Am. Chem. Soc.*, 2001, vol. 123, pp. 12085–86.
2. A.C. Roy and D. Mohanta: *Scripta Mater.*, 2009, vol. 61, pp. 891–94.
3. H.C. Pant, M.K. Patra, A. Verma, S.R. Vadera, and N. Kumar: *Acta Mater.*, 2006, vol. 54, pp. 3163–69.
4. P. Durán, F. Capel, J. Tartaj, D. Gutierrez, and C. Moure: *Sol. St. Ion.*, 2001, vol. 141, pp. 529–39.
5. Y. Kim and K. Ryu: *Curr. Appl. Phys.*, 2006, vol. 6S1, pp. 266–70.
6. W. Lu and M. Quilitz: *J. Eur. Ceram. Soc.*, 2007, vol. 27, pp. 3149–59.
7. D. Sarkar: *J. Am. Ceram. Soc.*, 2011, vol. 94, pp. 106–10.
8. F. Guangneng and H. Lixia: *J. Cryst. Growth*, 2005, vol. 279, pp. 489–93.
9. M.R. Mohammadi and D.J. Fray: *Particuology*, 2011, vol. 9, pp. 235–42.
10. V. Vinothini, P. Singh, and M. Balasubramanian: *Ceram. Int.*, 2006, vol. 32, pp. 99–103.
11. O.A. Harizanov: *Mater. Lett.*, 1998, vol. 34, pp. 232–36.
12. R. Ashiri and A. Nemati: *J. Non-Cryst. Solids*, 2009, vol. 355, pp. 2480–84.
13. R. Ashiri and A. Nemati: *Mater. Res. Bull.*, 2011, vol. 46, pp. 2291–95.
14. X. Xing, J. Deng, J. Chen, and G. Liu: *J. Alloy. Compd.*, 2004, vol. 384, pp. 312–17.
15. B. Lee and J. Zhang: *Thin Solid Films*, 2001, vol. 388, pp. 107–13.
16. C.R. Brundle, C.A. Evans, and J.S. Wilson: *Encyclopedia of Materials Characterization*, Butterworth-Heinemann, Boston, MA, 1992.
17. B. Cui and P. Yu: *Mater. Sci. Eng. B*, 2006, vol. 133, pp. 205–208.
18. M. Burgos and M. Langlet: *Thin Solid Films*, 1999, vol. 349, pp. 19–23.
19. S. Tangwiwat and S.J. Milne: *J. Non-Cryst. Solids*, 2005, vol. 351, pp. 976–80.
20. K.M. Hung, W.D. Yang, and C.C. Huang: *J. Eur. Ceram. Soc.*, 2003, vol. 23, pp. 1901–10.
21. O. Harizanov and A. Harizanova: *Mater. Sci. Eng. B*, 2004, vol. 106, pp. 191–95.
22. A. Ianculescu and M. Gartner: *Appl. Surf. Sci.*, 2006, vol. 253, pp. 344–48.
23. M. Sasani Ghamsari and A.R. Bahramian: *Mater. Lett.*, 2008, vol. 62, pp. 361–64.
24. L. Ramajo, R. Parra, and M. Reboredo: *Mater. Chem. Phys.*, 2008, vol. 107, pp. 110–14.
25. S. Ghosh, S. Dasgupta, and A. Sen: *Mater. Lett.*, 2007, vol. 61, pp. 538–41.
26. C.N. George and J.K. Thomas: *J. Mater. Charact.*, 2009, vol. 60, pp. 322–26.
27. E. Brzozowski and M.S. Castro: *J. Euro. Ceram. Soc.*, 2000, vol. 20, pp. 2347–51.
28. H.I. Hsiang and Y.L. Chang: *J. Alloy. Compd.*, 2011, vol. 509, pp. 7632–38.
29. F. Baeten and B. Derks: *J. Eur. Ceram. Soc.*, 2006, vol. 26, pp. 589–92.
30. U. Chaimongkon, A. Thongtha, and T. Bongkarn: *Curr. Appl. Phys.*, 2011, vol. 11, pp. S70–S76.
31. B.D. Cullity: *The Elements of X-Ray Diffraction*, 2nd ed., Addison Wesley, Boston, MA, 1978.
32. P. Yu and B. Cui: *Mater. Sci. Eng. A*, 2008, vol. 473, pp. 34–41.
33. R. Ashiri: M.Sc. Dissertation, Sharif University of Technology, Tehran, Iran, 2008.